Nanoscale

Cite this: *Nanoscale*, 2012, **4**, 4702

www.rsc.org/nanoscale

PAPER

Direct observation of melting behaviors at the nanoscale under electron beam and heat to form hollow nanostructures†

Chun-Wei Huang,[a] Cheng-Lun Hsin,[a] Chun-Wen Wang,[a] Fu-Hsuan Chu,[a] Chen-Yen Kao,[a] Jui-Yuan Chen,[a] Yu-Ting Huang,[a] Kuo-Chang Lu,[c] Wen-Wei Wu*[a] and Lih-Juann Chen*[b]

Received 26th March 2012, Accepted 25th May 2012
DOI: 10.1039/c2nr30724c

We report the melting behaviours of ZnO nanowire by heating ZnO–Al_2O_3 core–shell heterostructures to form Al_2O_3 nanotubes in an *in situ* ultrahigh vacuum transmission electron microscope (UHV-TEM). When the ZnO–Al_2O_3 core–shell nanowire heterostructures were annealed at 600 °C under electron irradiation, the amorphous Al_2O_3 shell became single crystalline and then the ZnO core melted. The average vanishing rate of the ZnO core was measured to be 4.2 nm s^{-1}. The thickness of the Al_2O_3 nanotubes can be precisely controlled by the deposition process. Additionally, the inner geometry of nanotubes can be defined by the initial ZnO core. The result shows a promising method to obtain the biocompatible Al_2O_3 nanotubes, which may be applied in drug delivery, biochemistry and resistive switching random access memory (ReRAM).

Introduction

Nanomaterials with remarkable mechanical, field emission, electrical, magnetic, optical and chemical properties have been extensively investigated.[1–4] At the nanoscale, the fundamental properties of bulk materials can change. One of the most prominent examples is the decrease in melting point of nanoparticles.[5,6] The effects of size on the melting temperature of metallic nanoparticles embedded in an insulating, high melting temperature matrix, such as Pb nanoparticles in amorphous SiO_2 or Al_2O_3 matrix, were investigated.[7] In addition, the electron beam irradiation was found to influence the structure modification of small Au particles,[8] due to the electron beam charging and heating of the nanoparticles. Several reports have addressed the importance of the irradiation of the high energy electrons,[9] which can cause the physical effects on nanostructures and lead to interesting results in technological applications of these nanosystems.

Metal oxides have attracted great attention in the past decades. Among them, Al_2O_3 is one of the most important materials for its potential applications in drug delivery, biochemistry,[10,11] optics,[12] resistive switching random access memory (ReRAM) and electronics. Several methods have been proposed to fabricate Al_2O_3 nanomaterials with a variety of geometries, such as nanoparticles, nanorods, nanowires and nanotubes.[13–15] Among them, the template-assisted method is representative for fabricating nanotubes. Generally, the fabrication process involves three steps: first, formation of the template; second, formation of the core–shell nanostructures; finally, removal of the templates for the designed geometry.[16] Porous anodic alumina,[17] alumina nanotubes,[18,19] cholesterol nanotubes[20] and carbon nanotubes[21–23] have been used as templates. Various methods to remove the template were also investigated. Therefore, the understanding of the removal process is essential for the design of more exquisite nanostructures. For example, ZnO reacted with ammonia[24] and hydrogen at high temperatures.[25] Yang *et al.*[26,27] had studied the irradiation-induced local etching mechanism. Meanwhile, for the purpose of direct examination, *in situ* transmission electron microscope (TEM) has been proven to be a powerful tool for atomic-level observation, including phase/shape transformation, molten nanofluidic migration and electromigration.[28–40] Here, we report the observation of the irradiation of ZnO–Al_2O_3 core–shell nanostructures to form the Al_2O_3 nanotubes in an ultra-high-vacuum transmission electron microscope (UHV-TEM). The ZnO nanostructures were used as templates and removed *via* electron irradiation to form the Al_2O_3 nanotube from the ZnO–Al_2O_3 core–shell nanostructure at 600 °C. The shell structure was formed by atomic layer deposition (ALD) process. A new formation mechanism has been proposed and the effect of heat and electron irradiation were identified by the *in situ* TEM observation.

[a]*Department of Materials Science and Engineering, National Chiao Tung University, No.1001, University Rd., East Dist., Hsinchu City 300, Taiwan. E-mail: wwwu@mail.nctu.edu.tw; Fax: +886-3-5724727; Tel: +886-3-5712121-55395*
[b]*Department of Materials Science and Engineering, National Tsing Hua University, Hsinchu 300, Taiwan. E-mail: ljchen@mx.nthu.edu.tw*
[c]*Department of Materials Science and Engineering National Cheng Kung University, Tainan 701, Taiwan*

† Electronic supplementary information (ESI) available: Proof of the electron irradiation effect and three *in situ* TEM videos as dynamic observation of the ZnO–Al_2O_3 core–shell nanowire heterostructures forming the Al_2O_3 nanotube at 600 °C under electron irradiation and the disappearance of the ZnO core. See DOI: 10.1039/c2nr30724c

Experimental

Here, single-crystalline ZnO nanowires were synthesized on a Si (100) substrate in a three-zone furnace using the carbothermal reduction method through the vapor–liquid–solid mechanism.[41–45] Before loading into the furnace, Au was deposited as catalysts with a high vacuum e-beam evaporator. Mixed powders of zinc oxide and carbon with a mass ratio of 2 : 1 was placed in an alumina boat at the high-temperature (950 °C) zone while the substrate was placed at the low temperature (750 °C) zone. The temperatures were elevated at the rate of 10 °C per min and held for 90 min. The furnace was then cooled down to room temperature. Argon and oxygen were introduced at flow rates of 100 and 10 sccm, respectively. The ZnO–Al_2O_3 core–shell nanostructure was prepared with an ALD system. 25 nm thick alumina was deposited at 250 °C with trimethylaluminum (TMA) as the source. The processing pressure of introducing the chemical precursors and Ar purging was 210 and 193 mTorr, respectively. In our processing, a total of 268 cycles was used, resulting in an alumina thickness of 25 ± 1 nm, which corresponds to an average growth rate of 0.093 nm per cycle. A field emission scanning electron microscope (FESEM) JEOL JSM-6500F was used to examine the morphology of core–shell nanowires. High-resolution lattice imaging and line scan were performed with a JEOL 2100F TEM equipped with an energy dispersive spectrometer (EDS). *In situ* TEM observations were carried out in a JEOL 2000V UHV-TEM, which has a base pressure of 3×10^{-10} Torr. During the *in situ* TEM observation, the temperature was raised to 600 °C to investigate the morphological change of the ZnO–Al_2O_3 core–shell nanowire heterostructure with electron beam irradiation. The *in situ* TEM was equipped with a video recorder with 1/30 s time resolution.

Results and discussion

Fig. 1 is the schematic illustration of the nanotube formation process. The as-synthesized ZnO nanowire in Fig. 1(a) is grown by the vapor–liquid–solid growth process. The first step is to form the core–shell nanostructure with an ALD system (from (a) to (b)). Al_2O_3 nanotubes could be achieved when the reaction temperature was raised to 600 °C by electron irradiation on the core–shell nanowire in the UHV-TEM. From Fig. 1(b) and (c), the core ZnO nanowire is shown to have vanished and the Al_2O_3 nanotube shell has crystallized.

A SEM image of the as-synthesized ZnO nanowires is shown in Fig. 2(a) and Fig. 2(b) depicts the high magnification SEM image of the as-synthesized ZnO nanowires in Fig. 2(a). The lengths of the nanowires are about 10–15 μm and the diameters of the nanowires are in the range of 45–55 nm. Fig. 2(c) shows the SEM image of ZnO–Al_2O_3 core–shell nanowires and Fig. 2(d) is the corresponding magnified SEM image. A distinct contrast of the core–shell can be seen. After 268 cycles of Al_2O_3 coating, the uniform shells around the ZnO nanowires are evident.

Fig. 3 shows TEM images and EDS spectra which reveal the composition and structure of the core–shell nanowire. In Fig. 3(a), the image shows a smooth interface between the core and shell. The [0001] growth direction of the NW was identified by the diffraction pattern and the zone axis is [1$\bar{2}$10]. Fig. 3(b) is the HRTEM image corresponding to Fig. 3(a). The HRTEM image indicates the crystallinity of the single-crystalline ZnO core and the amorphous Al_2O_3 shell. Both the fast Fourier transform diffraction pattern (FFTDP) in the inset of Fig. 3(a) and the lattice spacing in Fig. 3(b) show that the ZnO core is single crystalline. The energy-dispersive X-ray spectra (EDS) line scan across the wire confirmed the presence elements of Zn, Al and O with a core–shell distribution.

The images in Fig. 4 were taken from the *in situ* TEM video, revealing the melting and vanishing of the ZnO core. During the *in situ* observation, the samples were found to be sensitive to the electron irradiation and the resulting energy deposition would cause significant perturbations in the system, including collective charge oscillations and irreversible atomic displacement.[46] The electron irradiation on the core–shell nanowire is expected to give rise to energy transfer and heating of the nanowire. On the other hand, the Al_2O_3 shell with high melting temperature will withstand the heating, which melt the ZnO nanowire, like a heat barrier.[47] We can expect that a high interfacial energy between

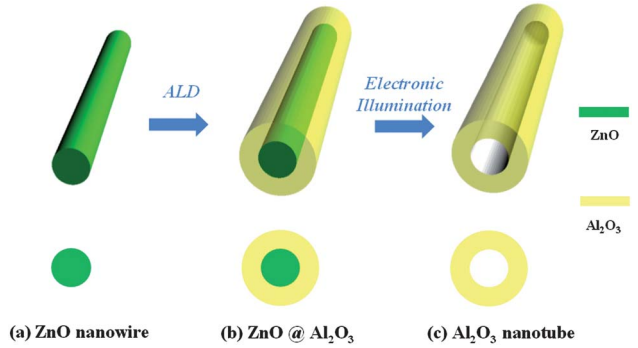

Fig. 1 Schematic illustration of the formation process of Al_2O_3 nanotubes. (a) Single-crystal ZnO nanowires grown by the vapor–liquid–solid mechanism, (b) ZnO–Al_2O_3 core–shell nanowires coated with a uniform Al_2O_3 layer by ALD, and (c) Al_2O_3 nanotubes formed by electron irradiation and heating.

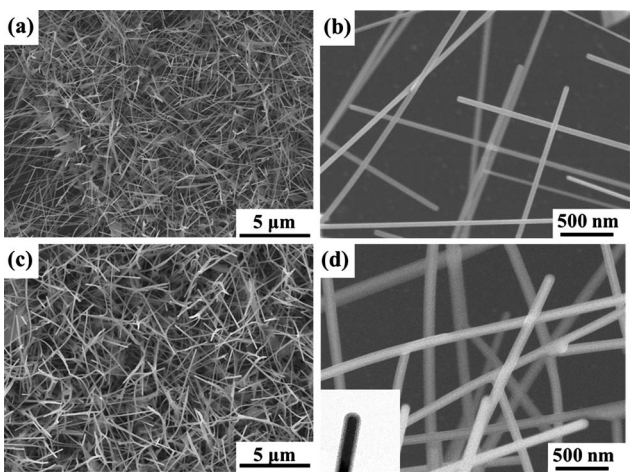

Fig. 2 (a) Low magnification and (b) high magnification SEM images of ZnO nanowires on the silicon substrate. (c) Low magnification and (d) high magnification SEM images of the ZnO–Al_2O_3 core–shell nanowires. Inset shows the ZnO core and Al_2O_3 shell with a sharp interface. The image contrast was reversed to highlight the core–shell structure.

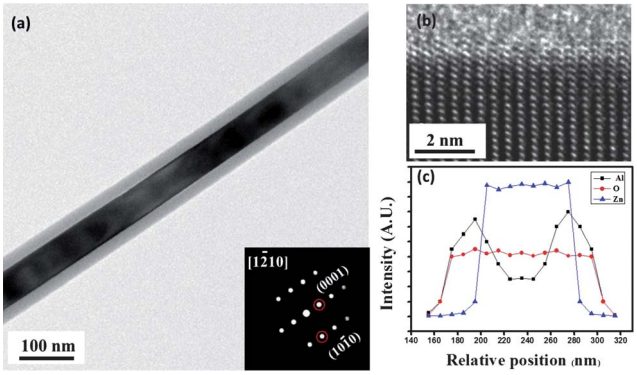

Fig. 3 (a) TEM image of a ZnO–Al_2O_3 core–shell nanowire. Inset shows the FFT diffraction pattern of the ZnO core. (b) A HRTEM image of the single crystalline ZnO core and the amorphous Al_2O_3 shell. (c) EDS line scan of the core–shell nanowire. The energy-dispersive X-ray spectra line scan across the nanowire also confirmed the presence of elements of Zn, Al and O with a core–shell distribution. Al shows a gorge-like intensity profile, being consistent with the core–shell nanostructure.

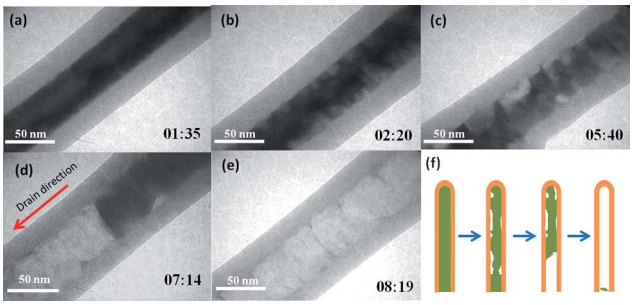

Fig. 4 A series of images showing the formation process. The melting occurred at the interface between the ZnO core and the Al_2O_3 shell. (a)–(c) Phase transition of ZnO from solid to liquid. (d) and (e) ZnO liquid drains away and the Al_2O_3 nanotube was formed. The remaining ZnO in the core was in the solid phase. (f) Schematic illustration of the formation process. First, the melting of ZnO occurs at the ZnO–Al_2O_3 interface; then the liquid ZnO drains away at the open end. Finally, the ZnO nanowire completely disappears and the empty Al_2O_3 nanotube is in place.

Al_2O_3 and ZnO could be the driving force of the observed reaction. Furthermore, the ZnO nanowire alone was intact under the same irradiation condition (ESI, Fig. S-1†). For comparison, we have designed an additional experiment to anneal ZnO–Al_2O_3 core–shell nanowires under the same heating conditions but without electron irradiation, for which no change was observed. The results from the series of experiments indicate that electron irradiation and the concurrent presence of the Al_2O_3 shell are crucial for the melting of the ZnO core.

For phase transition from solid to liquid,[48] based on the thermodynamic model for the prediction of melting point reduction of the solid phase, surface melting will occur at the surface tension transition point (ESI, Video-1†). This result is well coordinated with the report of size dependent melting of nanocrystals.[49] In Fig. 4(a), it is clear that the melting occurred at the interface between the ZnO core and the Al_2O_3 shell. When the ZnO surface layer became liquid, the droplet would coalesce to change the morphology to minimize the interfacial energy (Fig. 4(b) and (c)).

Since the ZnO–Al_2O_3 core–shell nanowire was detached from the substrate by ultrasonication, the ZnO–Al_2O_3 core–shell nanowire was broken at the bottom of the as-grown samples. Then the ZnO nanowire is enclosed by the Al_2O_3 shell with a opening at one end. The molten ZnO was drained by the chamber vacuum. Then the molten ZnO droplets receded very quickly along the length of the wire, leaving the coarse ZnO core empty and forming the nanotube. Therefore, the coarse ZnO core was formed (Fig. 4(c)). When the temperature was sufficient to melt the remaining ZnO core, the ZnO liquid is drained away quickly to the open side, as shown in Fig. 4(d). Eventually, the ZnO nanowire completely vanished, leaving the empty Al_2O_3 nanotube (Fig. 4(e)). When the liquid ZnO drained away at the open end, it was expected to find it accumulated at one end of the nanotube (ESI, Fig. S-2†). We believe that it is to balance the pressure between the region inside the tube and the outside vacuum environment. A schematic illustration depicting the reaction process is presented in Fig. 4(f) (the green part is ZnO and the other is Al_2O_3).

Fig. 5 shows the plot of the length of hollow portion as a function of reaction time. It is apparent that there are two different stages. The first stage corresponds to the heating and melting of the ZnO core under the electron irradiation. In the mean time, the Al_2O_3 shell functions as a protective cover to prevent the outflow of the ZnO as its temperature approaches the melting point. After 150 s of preheating, the vanishing rate of ZnO increased under electron irradiation. This is attributed to the fact that the ZnO core was liquidized completely, increasing the fluidity (ESI, Video-2†). Based on our results, the average vanishing rate of ZnO core has been measured to be 4.2 nm s^{-1}. Additionally, the ZnO core was liquidized and always disappeared along the [0001] growth direction, leaving clear and straight single crystalline Al_2O_3 nanotubes at high temperature (ESI, Video-3†).

The microstructure and composition of the nanotube were characterized by TEM. Fig. 6(a) shows the low magnification image of the Al_2O_3 nanotube, revealing the hollow structure. The

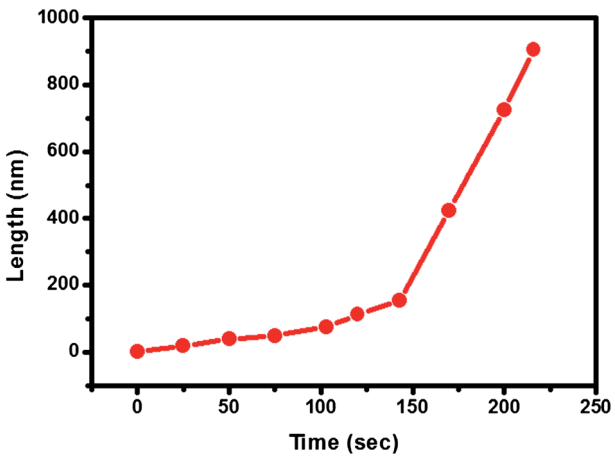

Fig. 5 Plot of the length of vanishing ZnO as a function of time. There are two different stages. The first stage corresponds to the heating and melting of the ZnO core under the electron irradiation. After 150 s of preheating, the vanishing rate of ZnO increased under electron irradiation.

EDS line scan in Fig. 6(a) explicitly shows the chemical distribution after the reaction. The intensity profile demonstrates the tubular Al_2O_3 structure and confirms the absence of Zn, indicating that the ZnO core has been completely removed and only Al_2O_3 nanotube remains. The HRTEM image in Fig. 6(b) depicts the crystalline structure of the Al_2O_3 nanotube, the $d_{(1\bar{1}1)} = 0.47$ nm and $d_{(002)} = 0.45$ nm. With electron irradiation at 600 °C for 10 min, the amorphous Al_2O_3 shell was crystallized. It was found that the Al_2O_3 nanotube could be formed under high intensity of irradiation at an appropriate heating temperature. Based on the computational modeling of the FFT diffraction pattern and crystal plane spacing from the HRTEM image, the alumina shell was confirmed to be of cubic phase.

The melting was found to be different from the previous report.[50–55] No Kirkendall effect between ZnO core and Al_2O_3 shell was detected in our work since the outer Al_2O_3 shell was intact. Otherwise, the outer shell could have the composition of $Zn_xAl_yO_z$ instead of Al_2O_3. Moreover, the electron irradiation effect was different from the report by Yang *et al.*[26] In their report, the shell of the nanotube was composed of original amorphous alumina and a number of embedded ZnO. In our result, single crystalline Al_2O_3 was formed and no Zn element found in the Al_2O_3 shell layer *via* local etching of the ZnO core by electron-beam irradiation. It is worthwhile to mention that the Al_2O_3 nanotube can be considered as a representative shell utilizing the ZnO nanowire as a template. A variety of ZnO nanostructures has been synthesized by a number of growth methods. It is feasible to fabricate clean, flat and hollow Al_2O_3 nanostructures by ALD on inner ZnO core with various geometries (ESI, Fig. S-3†). The controllable formation process will be essential in future applications of the nanoscale cylindrical capacitors, drug delivery and optical transmission.

Conclusions

In summary, we have fabricated single crystalline Al_2O_3 nanotube and investigated the interface melting of ZnO–Al_2O_3 core–shell structure under electron irradiation in UHV-TEM at 600 °C. The average vanishing rate of ZnO core was measured to be 4.2 nm s^{-1}. The geometry of Al_2O_3 nanotube can be controlled by the inner ZnO template. The amorphous Al_2O_3 nanostructure can become crystalline by the electron irradiation and heating. The study demonstrates a promising method to obtain the biocompatible Al_2O_3 hollow nanostructures, which may play a crucial role in nanomedicine, biochemistry, ReRAM and MEMS units in nanoelectronics.

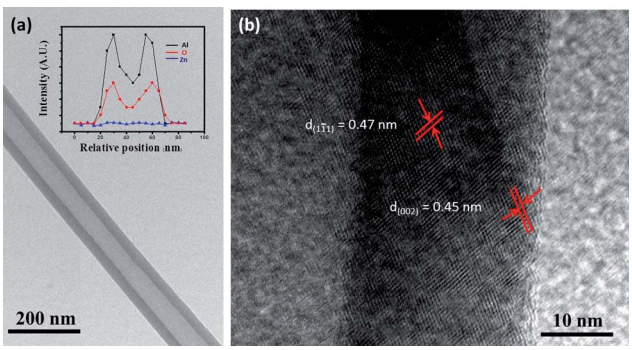

Fig. 6 (a) Low magnification TEM image of the Al_2O_3 nanotube. Inset is the EDS line scan of the Al_2O_3 nanotube. The intensity profile demonstrates the Al_2O_3 tubular structure and confirms the absence of Zn. (b) A HRTEM image of the Al_2O_3 nanotube. The amorphous Al_2O_3 shell was crystallized and has lattice constants $d_{(1\bar{1}1)} = 0.47$ nm and $d_{(002)} = 0.45$ nm.

Acknowledgements

W.W.W., L.J.C. and K.C.L. acknowledge the support by National Science Council through grants 100-2628-E-009-023-MY3, 99-2120-M-007-011, 98-2221-E-007-104-MY3, and 100-2628-E-006-025-MY2.

Notes and references

1 R. H. Baughman, A. A. Zakhidov and W. A. de Heer, *Science*, 2002, **297**, 787–792.
2 S. Yip, *Nature*, 1998, **391**, 532–533.
3 C. L. Hsin, W. Mai, Y. Gu, Y. Gao, C. T. Huang, Y. Liu, L. J. Chen and Z. L. Wang, *Adv. Mater.*, 2008, **20**, 3919–3923.
4 M. M. Adachi, M. P. Anantram and K. S. Karim, *Nano Lett.*, 2010, **10**, 4093–4098.
5 J. J. Thompson, *Application Dynamics to Physics and Chemistry*, MacMillan, London, 1888.
6 T. Yokota, M. Murayama and J. M. Howe, *Phys. Rev. Lett.*, 2003, **91**, 2655041.
7 E. Johnson, U. Dahmen, S. J. Chen and T. Fujii, *Mater. Sci. Forum*, 1999, **115**, 294–296.
8 D. J. Smith, A. K. Petford, L. R. Wallenberg and J. O. Bovin, *Science*, 1986, **233**, 872–875.
9 S. Xu, M. Tian, J. Wang, J. Xu, J. M. Redwing and M. H. W. Chan, *Small*, 2005, **1**, 1221–1229.
10 R. Kurz, A. Sickinger and A. Robitzki, in *World Congress on Medical Physics and Biomedical Engineering, September 7-12, 2009, Munich, Germany*, ed. O. Dössel and W. C. Schlegel, Springer, Berlin Heidelberg, 2009, vol. 25/8, pp. 95–97.
11 K. C. Popat, G. Mor, C. A. Grimes and T. A. Desai, *Langmuir*, 2004, **20**, 8035–8041.
12 X. S. Peng, L. D. Zhang, G. W. Meng, X. F. Wang, Y. W. Wang, C. Z. Wang and G. S. Wu, *J. Phys. Chem. B*, 2002, **106**, 11163–11167.
13 G. Cundiah, F. L. Deepak, A. Govindaraj and C. N. R. Rao, *Top. Catal.*, 2003, **24**, 137–146.
14 S. H. Oh, M. F. Chisholm, Y. Kauffmann, W. D. Kaplan, W. Luo, M. Rühle and C. Scheu, *Science*, 2010, **330**, 489–493.
15 Y. Qin, Y. Yang, R. Scholz, E. Pippel, X. Lu and M. Knez, *Nano Lett.*, 2011, **11**, 2503–2509.
16 H. W. Liang, S. Liu and S. H. Yu, *Adv. Mater.*, 2010, **22**, 3925–3937.
17 D. T. Mitchell, S. B. Lee, L. C. M. Trofin, N. Li, T. K. Nevanen, H. Söderlund and C. R. Martin, *J. Am. Chem. Soc.*, 2002, **124**, 11864–11865.
18 H. Ogihara, M. Sadakane, Y. Nodasaka and W. Ueda, *Chem. Mater.*, 2006, **18**, 4981–4983.
19 J. Hwang, J. S. L. Min, K. Keem, K. Y. Cho, M. Y. Sung, M. S. Lee and S. Kim, *Adv. Mater.*, 2004, **16**, 422–425.
20 J. H. Jung, S. H. Lee, J. S. Yoo, K. Yoshida, T. Shimizu and S. Shinkai, *Chem.–Eur. J.*, 2003, **9**, 5307–5313.
21 B. C. A. Satishkumar, E. M. Vogl, L. Basumallick and C. N. R. Rao, *Chem. Commun.*, 1997, 604–606.
22 B. C. Satishkumar, A. Govindaraj, M. Nath and C. N. R. Rao, *J. Mater. Chem.*, 2000, **10**, 2115–2119.
23 T. Druzhinina, S. Hoeppener and U. S. Schubert, *Adv. Mater.*, 2011, **23**, 953–970.
24 F. Hamdani, A. E. Botchkarev, H. Tang, W. Kim and H. Morkoc, *Appl. Phys. Lett.*, 1997, **71**, 3111.
25 J. Goldberger, R. He, Y. Zhang, S. Lee, H. Yan, H. J. Choi and P. Yang, *Nature*, 2003, **422**, 599–602.
26 Y. Yang, R. Scholz, A. Berger, D. S. Kim, M. Knez, D. Hesse, U. Gösele and M. Zacharias, *Small*, 2008, **4**, 2112–2117.

27 H. J. Fan, A. Lotnyk, R. Scholz, Y. Yang, D. S. Kim, E. Pippel, S. Senz, D. Hesse and M. Zacharias, *J. Phys. Chem. C*, 2008, **112**, 6770–6774.
28 H. C. Hsu, W. W. Wu, H. F. Hsu and L. J. Chen, *Nano Lett.*, 2007, **7**, 885–889.
29 L. J. Chen and W. W. Wu, *Mater. Sci. Eng., R*, 2010, **70**, 303–319.
30 Y. C. Chou, W. W. Wu, L. J. Chen and K. N. Tu, *Nano Lett.*, 2009, **9**, 2337–2342.
31 W. W. Wu, K. C. Lu, C. W. Wang, H. Y. Hsieh, S. Y. Chen, Y. C. Chou, S. Y. Yu, L. J. Chen and K. N. Tu, *Nano Lett.*, 2010, **10**, 3984–3989.
32 K. C. Lu, W. W. Wu, H. Ouyang, Y. C. Lin, Y. Huang, C. W. Wang, Z. W. Wu, C. W. Huang, L. J. Chen and K. N. Tu, *Nano Lett.*, 2011, **11**, 2753–2758.
33 L. Sun, F. Banhart, A. V. Krasheninnikov, J. A. Rodríguez-Manzo, M. Terrones and P. M. Ajayan, *Science*, 2006, **312**, 1199–1202.
34 H. Zheng, R. K. Smith, Y. W. Jun, C. Kisielowski, U. Dahmen and A. P. Alivisatos, *Science*, 2009, **324**, 1309–1312.
35 Z. W. Shan, G. Adesso, A. Cabot, M. P. Sherburne, S. A. S. Asif, O. L. Warren, D. C. Chrzan, A. M. Minor and A. P. Alivisatos, *Nat. Mater.*, 2008, **7**, 947–952.
36 K. C. Chen, W. W. Wu, C. N. Liao, L. J. Chen and K. N. Tu, *Science*, 2008, **321**, 1066–1069.
37 C. L. Hsin, W. W. Wu, L. W. Chu, H. C. Hsu and L. J. Chen, *CrystEngComm*, 2011, **13**, 3967–3970.
38 C. Y. Wen, M. C. Reuter, J. Bruley, J. Tersoff, S. Kodambaka, E. A. Stach and F. M. Ross, *Science*, 2009, **326**, 1247–1250.
39 B. J. Kim, J. Tersoff, S. Kodambaka, M. C. Reuter, E. A. Stach and F. M. Ross, *Science*, 2008, **322**, 1070–1073.
40 C. L. Hsin, W. F. Lee, C. T. Huang, C. W. Huang, W. W. Wu and L. J. Chen, *Nano Lett.*, 2011, **11**, 4348–4351.
41 Y. Yang, R. Scholz, H. J. Fan, D. Hesse, U. Gösele and M. Zacharias, *ACS Nano*, 2009, **3**, 555–562.
42 C. L. Hsin, S. Y. Yu and W. W. Wu, *Nanotechnology*, 2010, **21**, 485602.
43 A. L. Schmitt, J. M. Higgins, J. R. Szczech and S. Jin, *J. Mater. Chem.*, 2010, **20**, 223–235.
44 H. J. Fan, P. Werner and M. Zacharias, *Small*, 2006, **2**, 700–717.
45 S. A. Morin, M. J. Bierman, J. Tong and S. Jin, *Science*, 2010, **328**, 476–480.
46 D. B. Williams and C. Barry Carter, *Transmission Electron Microscopy: A Textbook for Materials Science*, New York and London, 2009.
47 Y. Lereah, R. Kofman, J. M. Pénisson, G. Deutscher, P. Cheyssac, T. B. David and A. Bourret, *Philos. Mag. B*, 2001, **81**, 1801–1819.
48 J. Maddox, *Nature*, 1987, **330**, 599–600.
49 A. N. Goldstein, C. M. Echer and A. P. Alivisatos, *Science*, 1992, **256**, 1425–1427.
50 H. J. Fan, M. Knez, R. Scholz, K. Nielsch, E. Pippel, D. Hesse, M. Zacharias and U. Gösele, *Nat. Mater.*, 2006, **5**, 627–631.
51 J. Park, H. Zheng, Y. Jun and A. P. Alivisatos, *J. Am. Chem. Soc.*, 2009, **131**, 13943–13945.
52 Y. D. Yin, R. M. Rioux, C. K. Erdonmez, S. Hughes, G. A. Somorjai and A. P. Alivisatos, *Science*, 2004, **304**, 711–714.
53 H. J. Fan, M. Knez, R. Scholz, D. Hesse, K. Nielsch, M. Zacharias and U. Gösele, *Nano Lett.*, 2007, **7**, 993–997.
54 H. J. Fan, Y. Yang and M. Zacharias, *J. Mater. Chem.*, 2009, **19**, 885–900.
55 Y. D. Yin, C. K. Erdonmez, A. Cabot, S. Hughes and A. P. Alivisatos, *Adv. Funct. Mater.*, 2006, **16**(11), 1389–1399.

